KIF15 nanomechanics and kinesin inhibitors, with implications for cancer chemotherapeutics

Bojan Milic[a,1], Anirban Chakraborty[b,1], Kyuho Han[c], Michael C. Bassik[c,d], and Steven M. Block[b,e,2]

[a]Biophysics Program, Stanford University, Stanford, CA 94305; [b]Department of Biology, Stanford University, Stanford, CA 94305; [c]Department of Genetics, Stanford University School of Medicine, Stanford University, Stanford, CA 94305; [d]Chemistry, Engineering, and Medicine for Human Health, Stanford University, Stanford, CA 94305; and [e]Department of Applied Physics, Stanford University, Stanford, CA 94305

Edited by Yale E. Goldman, University of Pennsylvania/Pennsylvania Muscle Institute, Philadelphia, PA, and approved April 4, 2018 (received for review January 22, 2018)

Eg5, a mitotic kinesin, has been a target for anticancer drug development. Clinical trials of small-molecule inhibitors of Eg5 have been stymied by the development of resistance, attributable to mitotic rescue by a different endogenous kinesin, KIF15. Compared with Eg5, relatively little is known about the properties of the KIF15 motor. Here, we employed single-molecule optical-trapping techniques to define the KIF15 mechanochemical cycle. We also studied the inhibitory effects of KIF15-IN-1, an uncharacterized, commercially available, small-molecule inhibitor, on KIF15 motility. To explore the complementary behaviors of KIF15 and Eg5, we also scored the effects of small-molecule inhibitors on admixtures of both motors, using both a microtubule (MT)-gliding assay and an assay for cancer cell viability. We found that (*i*) KIF15 motility differs significantly from Eg5; (*ii*) KIF15-IN-1 is a potent inhibitor of KIF15 motility; (*iii*) MT gliding powered by KIF15 and Eg5 only ceases when both motors are inhibited; and (*iv*) pairing KIF15-IN-1 with Eg5 inhibitors synergistically reduces cancer cell growth. Taken together, our results lend support to the notion that a combination drug therapy employing both inhibitors may be a viable strategy for overcoming chemotherapeutic resistance.

optical tweezers | single-molecule biophysics | mitotic spindle | ispinesib | filanesib

Kinesins are ATP-driven motor proteins that mediate a variety of intracellular processes by translocating along, or exerting forces against, microtubules (MTs) (1–5). Some 45 kinesin genes, categorized into 15 families, have been identified in the human and mouse genomes (5–7). Over the past two decades, discoveries revealing the roles of certain kinesin family members in cell division and cancer have led to targeting these kinesins with antimitotic drugs (3, 8, 9). Drug development efforts have focused, for the most part, on Eg5, a kinesin-5 family motor that plays a key role in organizing the spindle during early stages of mitosis (3, 10, 11).

Eg5, also known as KIF11 or KSP (12–14), is a tetrameric kinesin composed of two pairs of identical, N-terminal motor domains, or "heads," connected to the opposite ends of a common stalk, composed of antiparallel, coiled-coil dimers formed from four C-terminal domains (15–17). Each head carries an MT-binding site, which allows a single Eg5 motor to cross-link adjacent MTs (16, 18). This, coupled with the ability of Eg5 dimers to undertake processive motility toward the plus end of MTs (19, 20), enables Eg5 tetramers to slide apart antiparallel MTs (18). In particular, Eg5 can slide apart MTs emanating from the twin centrosomes, thereby segregating these to the opposite poles of a cell and establishing spindle polarity along the axis of cell division (4, 10, 11, 14, 18, 19, 21–23). The role of Eg5 in mitotic spindle assembly has been highlighted by studies showing that bipolar spindles fail to form when Eg5 is either inhibited or absent (14, 19, 24).

Because Eg5 loss or inhibition prevents cell division, small-molecule drugs targeting Eg5 are candidates for chemotherapeutic agents. Academic and private-sector laboratories have pursued the development of dozens of Eg5 inhibitors (3, 8, 9). Despite these efforts, however, frontline chemotherapies incorporating kinesin inhibitors have failed to materialize, and no single drug has progressed beyond clinical trials to date (3, 8, 9).

A reason behind the failure of Eg5 inhibitors in cancer therapy is that a fraction of cells in tumors seem to be able to use a different kinesin motor, namely KIF15, to compensate for the loss of Eg5, fostering the development of drug resistance (3, 25–29). KIF15 is a kinesin-12 motor, also known as Hklp2 (30, 31): It is a plus end-directed MT motor whose oligomerization state appears to be salt-dependent. KIF15 has been isolated in both dimeric and tetrameric forms, depending on the ionic strengths of buffers used during purification (32–36). Each KIF15 polypeptide chain is composed of a conserved N-terminal motor domain and a C-terminal region that dimerizes into a coiled-coil stalk (Fig. 1*A* and *SI Appendix*, Fig. S1*A*). In addition to the MT-binding site present in each head, KIF15 polypeptides carry a second, noncatalytic MT-binding domain in the stalk region, which enables both dimeric and tetrameric forms of KIF15 to cross-link MTs (33, 34). Although KIF15, like Eg5, is capable of sliding apart MTs (33), both parallel (34) and antiparallel (36) mechanisms have been entertained.

During the normal course of mitosis, KIF15 preferentially binds to kinetochore MTs: spindle MTs whose plus ends are attached to kinetochores (26, 28). Despite being mainly a cytoplasmic protein, KIF15 localizes to the spindle after nuclear envelope breakdown (NEB) during prometaphase (25, 26, 28).

Significance

Eg5, a mitotic kinesin, has long been an anticancer drug target. However, a different kinesin motor, KIF15, can rescue cell division when Eg5 is incapacitated, leading to chemotherapeutic resistance. We characterized KIF15 motor mechanics at the single-molecule level and studied the effects of combinations of small-molecule inhibitors of KIF15 and Eg5 on admixtures of motors in a motility assay, as well as on cancer cell proliferation. Taken together, our results point the way toward a strategy of combination drug therapy targeting both Eg5 and KIF15 as a means of overcoming KIF15-mediated cancer resistance. This work highlights the importance of understanding the molecular physiology of different kinesins and of exploring inhibitors that target additional mitotic kinesins.

Author contributions: B.M. initiated the study; B.M. and A.C. generated and expressed recombinant kinesin constructs, carried out optical-trapping and MT-gliding experiments, and analyzed data; K.H. carried out the cell-viability experiments; M.C.B. and S.M.B. supplied guidance and supervision; and B.M., A.C., and S.M.B. wrote the paper.

The authors declare no conflict of interest.

This article is a PNAS Direct Submission.

[1]B.M. and A.C. contributed equally to this work.

[2]To whom correspondence should be addressed. Email: sblock@stanford.edu.

This article contains supporting information online at www.pnas.org/lookup/suppl/doi:10.1073/pnas.1801242115/-/DCSupplemental.

Published online April 27, 2018.

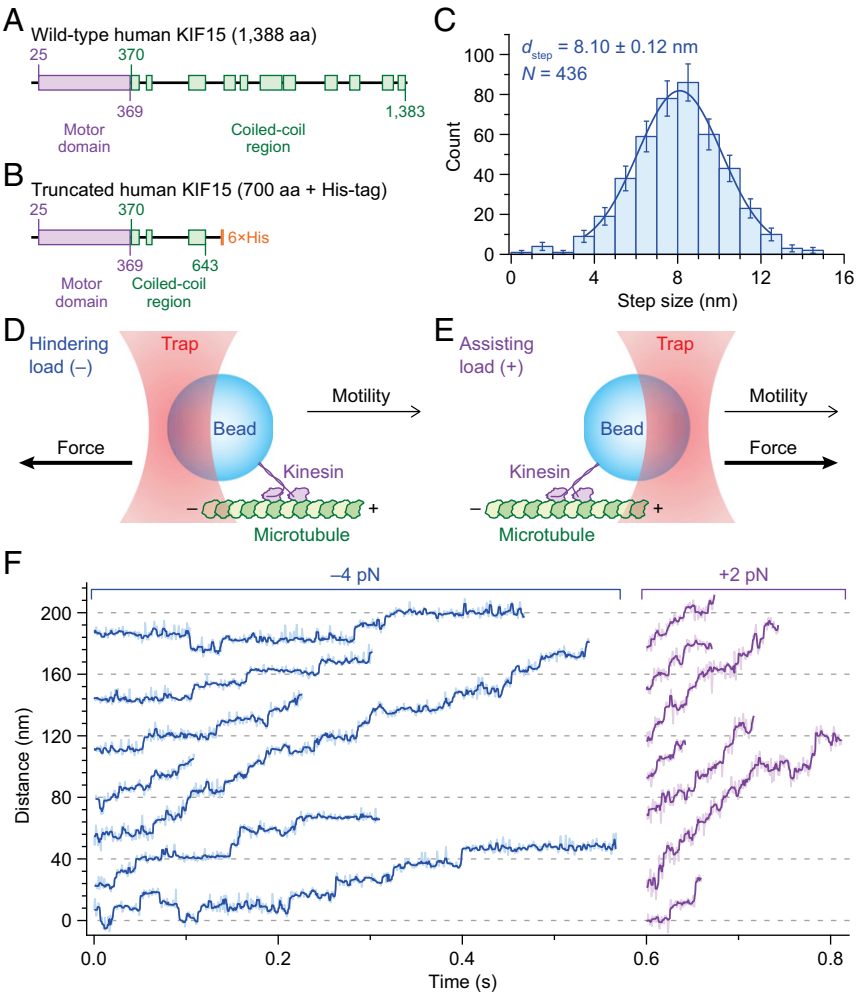

Fig. 1. Optical force-clamp assay for KIF15. Polypeptide representations of KIF15 show motor domains (purple), coiled-coil regions (green) identified by COILS scores (43) (*SI Appendix*, Fig. S1), and a 6× His-tag (orange) of the full-length human KIF15 (*A*; 1,388 aa) and the truncated construct used in this study (*B*; 700 aa). (*C*) Histogram of measured KIF15 step sizes (n = 436) under a 4-pN hindering load in saturating ATP (2 mM ATP; error bars indicate counting errors), with superposed Gaussian (solid line) and fitted mean step size, d_{step} (mean ± SE). A schematic depicts the experimental geometry of the optical-trapping assay (not to scale), showing arrangements for hindering load (*D*; –) and assisting load (*E*; +); directions of kinesin motion (light arrows) and applied load (heavy arrows) are indicated. (*F*) Representative records of individual KIF15 trajectories obtained under hindering (–4 pN; blue) or assisting (+2 pN; purple) loads at saturating ATP. Median-filtered traces (dark colors; seven-point sliding window) are superposed on the unfiltered data (pale colors).

Although the mechanism of KIF15 recruitment remains an active area of investigation, it is thought that TPX2, a nuclear protein released into the cytoplasm after NEB, facilitates the localization of KIF15 by bundling kinetochore MTs in a configuration favorable for KIF15 binding (33, 35, 37–39). In contrast, Eg5 begins associating with the spindle earlier, during prophase (before NEB), and is known to bind primarily to nonkinetochore MTs called interpolar MTs: antiparallel MTs that connect the spindle poles (19, 23, 40).

The rescue of cell division by KIF15 under conditions of Eg5 inhibition relies on the intracellular mislocalization of KIF15 to nonkinetochore MTs to an extent sufficient to establish spindle bipolarity, which is required for mitosis to proceed (25–29). Investigations of cancer cell lines have found that KIF15-mediated resistance occurs via one of two mechanisms: (*i*) KIF15 overexpression, facilitating greater occupancy on nonkinetochore MTs (25, 26, 28), or (*ii*) mutations in Eg5 motors that cause these to cross-link nonkinetochore MTs into bundles, which become conducive to KIF15 recruitment (29). Recent evidence suggests that KIF15 may be indispensable for resistance to Eg5 inhibitors: HeLa cells with knocked-down KIF15 expression seem incapable of developing resistance to Eg5 inhibitors (29).

Whereas Eg5 has been characterized extensively in bulk and at the single-molecule level (11, 41), our understanding of KIF15 motility is comparatively limited: In particular, the mechanochemical cycle of KIF15 and its properties relevant to mitosis, including processivity and MT dissociation rate under load, have remained incompletely characterized (32–36). Here, we applied single-molecule optical-trapping techniques to investigate the nanomechanics of the human KIF15 motor across a broad range of loads and ATP concentrations. Dozens of Eg5 inhibitors have been identified in screens, patented, and tested in the clinic (3), whereas a single patent application has been filed for an inhibitor of KIF15 (42), and no reports characterizing this inhibitor have yet appeared in peer-reviewed literature. Here, we implemented MT-gliding and cell-viability assays to characterize KIF15-IN-1, a KIF15 inhibitor that recently became available commercially, and we evaluated its effects when paired with one of two well-characterized Eg5 inhibitors: ispinesib (SB-715992) and filanesib (ARRY-520). We find that KIF15 motor behavior is substantially different from Eg5: KIF15 is up to sixfold faster but significantly less processive over the full range of loads, with an MT dissociation rate that is an order of magnitude greater. MT gliding

powered by admixtures of KIF15 and Eg5 motors is highly robust and ceases only when both motors are separately inhibited using different drugs. Finally, the data show that KIF15-IN-1 is a potent inhibitor of KIF15 motility that can act synergistically with Eg5 inhibitors to impair cancer cell proliferation. Taken together, our results suggest a strategy for countering KIF15-mediated chemotherapeutic resistance that involves combination treatment with both forms of kinesin inhibitor.

Results

KIF15 Is Processive Under Hindering and Assisting Loads. To investigate the behavior of dimeric KIF15 under load, we expressed a truncated construct encoding the first 700 amino acids (aa) of wild-type human KIF15 with a C-terminal 6× His-tag (Fig. 1*B* and *SI Appendix*, Fig. S1*B*). The polypeptide chain of this recombinant motor, hereafter referred to as KIF15, contains the complete N-terminal motor domain along with a significant portion of the coiled-coil stalk (43). Consistent with findings from other kinesin motors (20, 44–50), single molecules of KIF15 take ∼8-nm steps (Fig. 1*C*) and execute processive motility under both hindering (−) and assisting (+) external loads (Fig. 1 *D*–*F*).

KIF15 Is Faster than Eg5 Across Loads and ATP Concentrations. To evaluate KIF15 behavior under controlled external loads, we characterized its motility in the single-molecule limit over a range of applied loads and ATP concentrations using an optical force clamp in conjunction with a moving-bead assay (45, 47, 51–53). These data are juxtaposed with earlier data on a truncated form of human Eg5 (Fig. 2 and *SI Appendix*, Fig. S2), hereafter referred to as Eg5 (20, 54). We found that KIF15 was significantly faster than Eg5 across all loads and ATP conditions examined (Fig. 2 *A* and *C* and *SI Appendix*, Fig. S2*A*). KIF15 was also more sensitive to external forces than Eg5, and could be appreciably slowed down, or sped up, by the application of just a few piconewtons of hindering or assisting load, respectively. Although KIF15 and Eg5 velocities differ significantly, the load dependence of their randomness, a statistical measure of the regularity of step timing (55), was similar (Fig. 2 *B* and *D* and *SI Appendix*, Fig. S2*B*), indicating that these motors have similar numbers of rate-limiting transitions in their respective mechanochemical cycles.

Mechanochemical Cycles of KIF15 and Eg5. The characteristics of any molecular motor are governed by its mechanochemical cycle. Understanding the differences between KIF15 and Eg5 behavior under load (Fig. 2) therefore requires a quantitative characterization of this cycle for each motor. We modeled the single-molecule datasets for KIF15 and Eg5 (Fig. 2 and *SI Appendix*, Fig. S2 *A* and *B*) using a minimal, four-state kinetic scheme (Fig. 3*A*) whose transitions correspond to established biochemical and mechanical events comprising the kinesin cycle (50) (Fig. 3*B*).

The first kinetic transition of this scheme, from states [1] → [2], represents reversible ATP binding (53) to the nucleotide-free (apo), MT-bound head of a one-head-bound (1-HB) kinesin in the so-called ATP-waiting state (48, 56, 57). This transition, associated with the rates for ATP binding (k_1[ATP]) and ATP release (k_{-1}), is followed by the single, load-dependent transition of the kinesin cycle, from state [2] → [3]. This mechanical transition corresponds to partial docking of the neck linker (NL) to the MT-bound head (47). Recent single-molecule and structural evidence indicates that partial NL docking likely corresponds to a shift in the equilibrium between the fully docked and undocked states (47, 58, 59), advancing the average position of the ADP-bound, tethered head, and effectively repositioning it in front of the MT-bound head. Transition [2] → [3] is modeled by $k_2(F) = k_2^0 \exp[F\delta_2/k_BT]$, where k_2^0 is the unloaded rate constant, F is the applied load, δ_2 is a characteristic distance parameter, and k_BT is Boltzmann's constant times the absolute temperature. ATP hydrolysis then completes NL docking (47), which enables the tethered head to bind the MT, releasing ADP in the process and ultimately advancing the dimer by ∼8 nm. In the minimal model, these events have been combined into a single transition, [3] → [4], associated with the rate constant, k_3. Finally, the trailing head undergoes transition [4] → [1], associated with the rate constant, k_4, which entails releasing inorganic phosphate

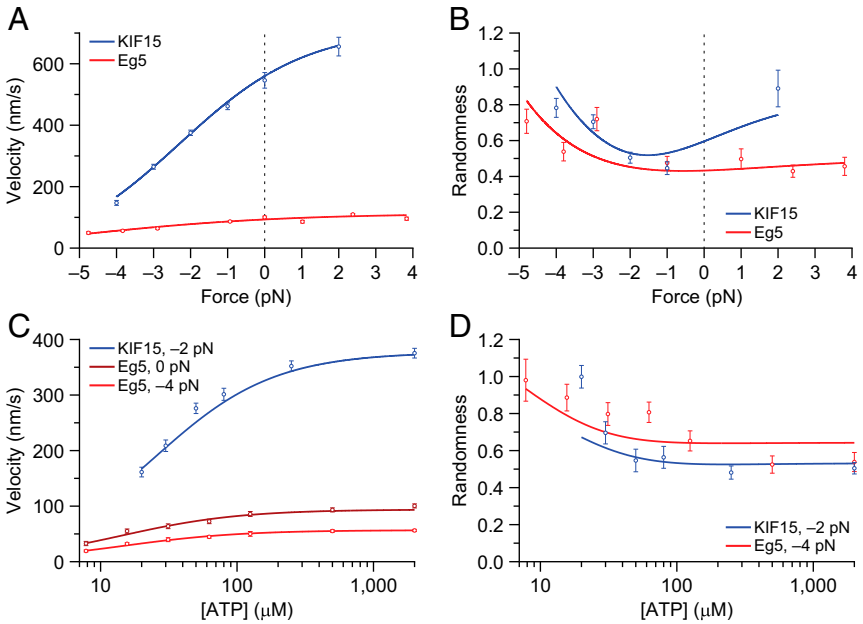

Fig. 2. Single-molecule motility of KIF15 and Eg5 under load. Velocity (*A*) and randomness (*B*) are shown as functions of applied load under saturating ATP conditions (open circles; mean ± SE) for KIF15 (blue; n = 79–247) and Eg5 (red; n = 62–212). Velocity (*C*) and randomness (*D*) are shown as functions of the ATP concentration (open circles; mean ± SE) for KIF15 (blue; n = 78–247; F = −2 pN) and Eg5 (red; n = 22–92; F = 0 pN and F = −4 pN). Solid lines in all panels represent global fits to the four-state model of Fig. 3. Eg5 data (but not model fits) are replotted from a study by Valentine et al. (20).

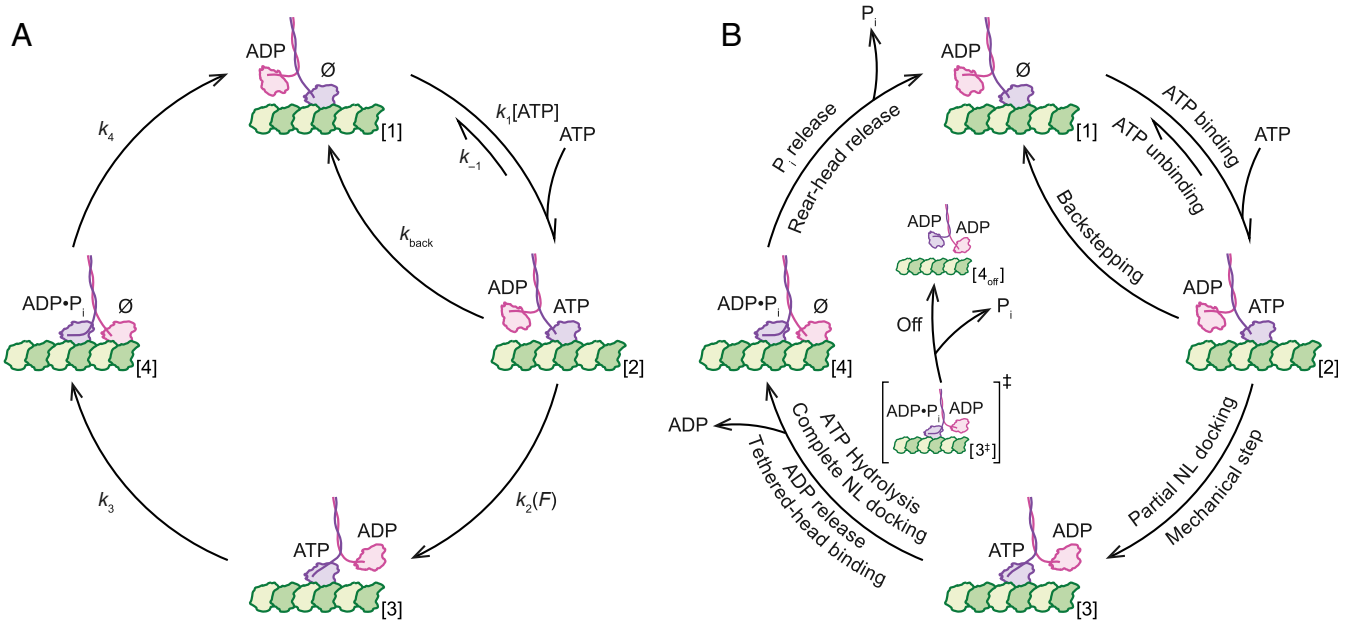

C

Parameter	Parameter description	KIF15	Eg5
k_1[ATP]	ATP binding	10.6 ± 2.4 $\mu M^{-1}s^{-1}$	0.98 ± 0.09 $\mu M^{-1}s^{-1}$
k_{-1}	ATP unbinding	477 ± 157 s^{-1}	12 ± 5 s^{-1}
k_2^0	Partial NL docking; Mechanical step	342 ± 42 s^{-1}	85 ± 19 s^{-1}
δ_2	Distance parameter	2.36 ± 0.13 nm	1.45 ± 0.16 nm
k_3	ATP hydrolysis; Complete NL docking; ADP release; Tethered-head binding	94 ± 5 s^{-1}	24 ± 3 s^{-1}
k_4	P_i release; Rear-head release	1,240 ± 580 s^{-1}	33 ± 8 s^{-1}
k_{back}	Backstepping	4.7 ± 1.0 s^{-1}	3.3 ± 0.5 s^{-1}

Fig. 3. Mechanochemical cycles of KIF15 and Eg5. (*A*) Minimal four-state kinetic representation of the kinesin mechanochemical cycle, based on a study by Milic et al. (50). (*B*) Transitions in the four-state scheme are assigned to specific biomechanical events by the partial NL-docking model. The first kinetic transition of this scheme, [1] → [2], represents reversible ATP binding to the nucleotide-free (Ø) MT-bound head of a 1-HB kinesin in the ATP-waiting state. This transition, associated with the rates for ATP binding (k_1[ATP]) and ATP release (k_{-1}), is followed by the single, load-dependent transition of the kinesin cycle, [2] → [3]. This mechanical transition, modeled by a force-dependent rate, $k_2(F)$, corresponds to partial docking of the NL to the MT-bound head. ATP hydrolysis then completes NL docking, which enables the tethered head to bind the MT, releasing ADP in the process, and ultimately advancing the dimer by ∼8 nm. In the minimal model, these events have been combined into a single transition, [3] → [4], associated with the rate constant, k_3. This composite transition implies passage through a 1-HB, posthydrolysis state, [$3^‡$], from which either (*i*) the tethered head binds the MT, [$3^‡$] → [4], thereby allowing the motor to continue stepping along the MT, or (*ii*) the bound head prematurely hydrolyzes ATP, leading to dissociation from the MT, [$3^‡$] → [4_{off}]. Finally, the trailing head undergoes transition [4] → [1], associated with the rate constant, k_4, which entails releasing P_i and detaching from the MT, thereby returning the dimer to the 1-HB ATP-waiting state. The four-state scheme also incorporates a back-stepping transition, k_{back}. In both panels, the nucleotide states of each head (purple/pink) are indicated as the dimer moves along the MT (green). ADP•P_i indicates heads in the posthydrolysis state. (*C*) Model parameters (rates and distances; mean ± SE) obtained by global fits to velocity and randomness measurements for KIF15 (blue) and Eg5 (red), based on the kinetic scheme in *A* (also Fig. 2 and *SI Appendix*, Fig. S2 *A* and *B*).

(P_i) and detaching from the MT, thereby returning the dimer to its original, 1-HB ATP-waiting state (60). The four-state scheme also incorporates a back-stepping transition leaving state [2], modeled by k_{back}, to accommodate increased randomness values that stem from occasional rearward steps (55).

Global fits to the KIF15 and Eg5 datasets (Fig. 2 and *SI Appendix*, Fig. S2 *A* and *B*) using analytical expressions for velocity and randomness (*Materials and Methods*) allowed us to determine values for all kinetic parameters (Fig. 3*C*). Surprisingly, the rates of all transitions in the KIF15 forward cycle were found to be significantly faster than the corresponding rates for Eg5, ranging from a factor of 4 up to two orders of magnitude. Only the back-stepping rates were found to be comparable. Under unloaded, saturating-ATP conditions, the ATP hydrolysis rate (k_3) represents the slowest rate in the cycle for both motors. For the case of Eg5, the rear-head release rate (k_4) is roughly comparable to the ATP hydrolysis rate (i.e., $k_{4,Eg5} \approx k_{3,Eg5}$). For KIF15, however, rear-head release is roughly 10-fold faster than hydrolysis (i.e., $k_{4,KIF15} \gg k_{3,KIF15}$). The characteristic distance parameter, δ_2, which determines the sensitivity of the motor to applied loads, is >60% higher for KIF15 than Eg5, consistent with the finding that the KIF15 force–velocity relationship is much steeper than that of Eg5.

ATP Hydrolysis Precedes Completion of the KIF15 Step. A feature of the partial-docking scheme that distinguishes it from alternative representations of the kinesin cycle (53, 61, 62) is that ATP binding incompletely docks the NL, so that the mechanical step is completed only after ATP hydrolysis, which leads to full NL docking (47). Thus far, the nanomechanics of kinesin-1 (47, 48,

58, 59), kinesin-2 (50), and Eg5 (63) have been shown to be consistent with the partial-docking mechanism.

To test the applicability of the partial-docking scheme to KIF15, we investigated how its run length (RL), the distance a single motor travels before MT dissociation, is affected by nucleotide conditions. The RL is governed by a competition between (*i*) processive advance, which is determined by the rate at which the motor enters the two-head-bound (2-HB) state, $[3^{\ddagger}] \rightarrow [4]$, and (*ii*) dissociation from the MT due to premature P_i release from the MT-bound head, $[3^{\ddagger}] \rightarrow [4_{off}]$ (Fig. 3*B*). Because the RL-determining transitions occur subsequent to ATP hydrolysis, $[3] \rightarrow [3^{\ddagger}]$, reducing either the rate of ATP binding (by reducing the ATP concentration) or ATP hydrolysis (by replacing ATP with a slowly hydrolyzed analog, ATPγS) would not be expected to affect the RL. As before (47, 48, 50), RLs were measured under low assisting loads (+2 pN) to avoid placing undue load on the front, unbound head, and to minimize perturbations to mechanical transitions in the MT-bound head. We found that the KIF15 RLs remained unchanged in response to reducing the rates of ATP binding (Fig. 4*A* and *SI Appendix*, Fig. S2*C*) or ATP hydrolysis (Fig. 4*A*).

KIF15 Is Less Processive than Eg5. We also investigated how RLs under different loads and ATP concentrations compared with Eg5 (Fig. 4*B* and *SI Appendix*, Fig. S2*C*). KIF15 was significantly less processive than Eg5 across all of the loads studied. KIF15 dissociation rates (Fig. 4*C*), computed by dividing the velocity (Fig. 2*A*) by the RL (Fig. 4*B*) under identical loading conditions, were an order of magnitude greater than the corresponding Eg5 rates for all loads.

KIF15 Rescues MT Gliding When Eg5 Is Fully Inhibited. We conducted MT-gliding assays (Fig. 5*A*) to evaluate the effect of the KIF15 inhibitor, KIF15-IN-1 (Fig. 5*B*), on transport by KIF15 and Eg5, and also when paired with one of two Eg5 inhibitors: ispinesib (Fig. 5*C*) and filanesib (Fig. 5*D*). To determine inhibitor levels required to abolish movement, we measured MT-gliding velocity as a function of inhibitor concentration, powered either by KIF15 or Eg5 alone (Fig. 5*E*). We found that 60 μM KIF15-IN-1 was sufficient to eliminate KIF15-based motility and that 1 μM ispinesib or filanesib was sufficient to eliminate Eg5-based motility. Even at these concentrations, which exceed the IC_{50} values by more than an order of magnitude (Fig. 5*F*), the effects of the inhibitors were motor-specific: MT gliding powered by Eg5 motors alone was unaffected by KIF15-IN-1 (Fig. 5*G*, red), and MT gliding powered by KIF15 motors alone remained unchanged in the presence of ispinesib or filanesib (Fig. 5*G*, blue).

In gliding assays powered by admixtures of KIF15 and Eg5 motors, we found that inhibiting just one of the two motors was insufficient to arrest MT motion (Fig. 5*G*, purple). KIF15 was able to maintain gliding even at concentrations of Eg5 inhibitor sufficiently high to inactivate all Eg5 motors. Similarly, Eg5 supported MT gliding in the presence of fully inactivated KIF15 motors, albeit at reduced velocity. These results held across the entire range of KIF15-to-Eg5 ratios explored (Fig. 5*H*), and KIF15 maintained MT gliding even when outnumbered nearly 10:1 by fully inhibited Eg5 motors. Gliding ceased only when KIF15-IN-1 plus either ispinesib or filanesib was present.

KIF15-IN-1 Acts Synergistically with Eg5 Inhibitors to Reduce Cancer Cell Viability. To assess potential synergistic effects of kinesin inhibitors in cancer cells, we treated HeLa cells in culture with varying levels of KIF15-IN-1 and ispinesib (Fig. 6*A*) or filanesib (Fig. 6*F*) and monitored survival after 72 h. We found that KIF15-IN-1 interacted synergistically with either Eg5 inhibitor to reduce cell number (Fig. 6 *B–D* and *G–I*), as assessed by the Bliss independence model (64, 65). Drug synergy was most pronounced for 20 μM KIF15-IN-1 in combination with 1 nM of either Eg5 inhibitor (Fig. 6 *E* and *J*).

Scoring HeLa cell survival using either fluorescence-based or non–fluorescence-based methods (*Materials and Methods*) yielded comparable results (Fig. 6 and *SI Appendix*, Fig. S4). The reduction in cell viability in response to the presence of ispinesib at nanomolar concentrations (Fig. 6*A*) compares favorably with previously reported LD_{50} measurements for ispinesib across a range of cancer cell lines, including HeLa cells (66, 67).

Discussion

Despite their ability to complement one another functionally, single-molecule measurements revealed dramatic differences in the nanomechanics of KIF15 and Eg5. These differences stem from large disparities in the mechanochemical cycle: All but a single one of the fitted transitions in the kinesin cycle are significantly faster for KIF15 than for Eg5 (Fig. 3*C*). KIF15 leaves the 2-HB state at a rate that is an order of magnitude faster than its slowest transition ($k_4 \gg k_3$), indicating that KIF15 remains bound by a single head throughout most of the stepping cycle. By contrast, Eg5 spends a substantial portion of its cycle with both heads bound, as established by previous biochemical work (68) and by our finding here that the rate for exiting the 2-HB state is comparable to the slowest transition in the cycle ($k_4 \approx k_3$). Because the simultaneous release of both heads from the MT is improbable, a motor in the 2-HB state has a much lower MT-dissociation rate than a motor in the 1-HB state. The

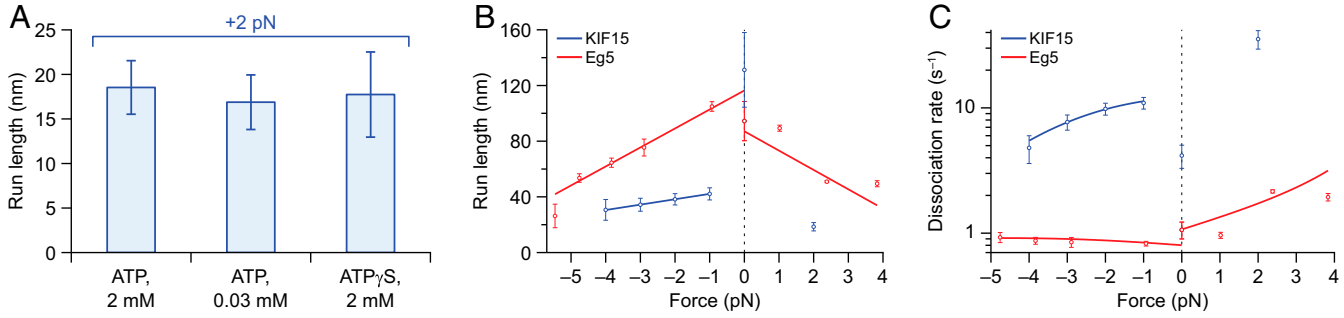

Fig. 4. Single-molecule KIF15 and Eg5 processivity. (*A*) KIF15 RL (bars; mean ± SE; $n = 47–144$) under a +2-pN load in the presence of ATP or ATPγS at the indicated concentrations. No statistically significant change occurred in response to varying the ATP concentration or replacing it by ATPγS. (*B*) Measurements of RL as a function of applied load at saturating ATP (open circles; mean ± SE) for KIF15 (blue; $n = 79–247$) and Eg5 (red; $n = 11–277$). Linear fits (solid lines) are shown. The Eg5 data (but not the fits) are replotted from a study by Valentine and Block (54) (also *SI Appendix*, Fig. S2*C*.). (*C*) MT dissociation rates as functions of applied load (open circles; mean ± SE) for KIF15 (blue; $n = 79–247$) and Eg5 (red; $n = 11–277$). Dissociation rates as functions of load were modeled (solid lines) by dividing the fit values of the velocity (Fig. 2*A*) for KIF15 (blue) or Eg5 (red) by the fit values of the RL at the corresponding forces in *B*.

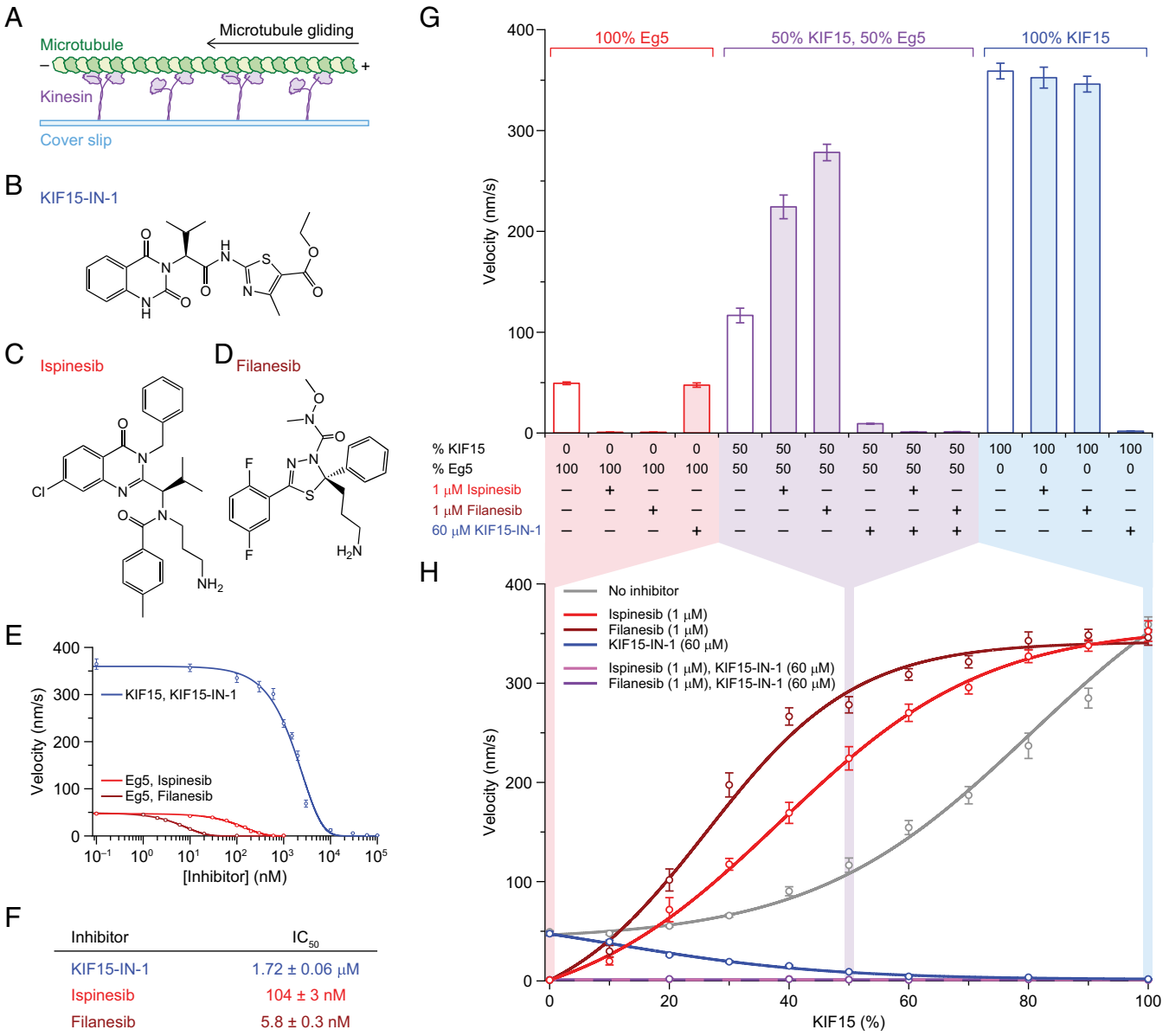

Fig. 5. MT gliding by KIF15 and Eg5 in the presence of inhibitors. (*A*) Cartoon representation of the gliding assay (not to scale): MTs (green) are transported by kinesin motors (purple) attached via their stalks to a glass coverslip (blue) (*Materials and Methods*). The chemical structures of KIF15-IN-1 (*B*), ispinesib (*C*), and filanesib (*D*) are shown. (*E*) MT-gliding velocities (open circles; mean ± SE) generated by KIF15 in the presence of KIF15-IN-1 (blue; $n = 14–31$) and Eg5 in the presence of ispinesib (red; $n = 9–30$) or filanesib (dark red; $n = 16–27$) as functions of inhibitor concentration. Solid lines are exponential fits. (*F*) Table of IC_{50} values (mean ± SE) from *E*. (*G*) MT-gliding velocities (mean ± SE) in the presence (shaded bars) or absence (open bars) of inhibitors, at the indicated concentrations, by Eg5 (red; $n = 12–25$), KIF15 (blue; $n = 19–23$), or both motors (purple; $n = 16–35$) (also *SI Appendix*, Fig. S3). (*H*) MT-gliding velocities (open circles; mean ± SE) generated by mixtures of motors. The KIF15-to-Eg5 motor ratio is expressed as the percentage of KIF15. Velocities were measured in the presence or absence of inhibitors at the concentrations indicated: no inhibitors (gray; $n = 15–56$), ispinesib (red; $n = 12–52$), filanesib (dark red; $n = 21–37$), KIF15-IN-1 (blue; $n = 21–32$), or KIF15-IN-1 with either ispinesib (light purple; $n = 14–20$) or filanesib (dark purple; $n = 15–19$). Sigmoidal (solid lines) and linear fits (dashed lines) are shown. Shaded backgrounds match the corresponding data in *G* and *H*, where inhibitor concentrations were chosen to be sufficient to fully inhibit the target motor, based on the data in *E*.

comparatively limited occupancy of the 2-HB state for KIF15 is therefore consistent with the finding that its dissociation rate is an order of magnitude higher than Eg5 across all loads (Fig. 4*C*).

Despite obvious disparities, the mechanochemical cycles of both KIF15 and Eg5 can be represented by a minimal, four-state kinetic scheme, albeit with very different transition rates. On this basis, we conclude that KIF15, like Eg5 (63), follows the partial NL-docking model of the mechanochemical cycle (47). This cycle is therefore not limited to processive transporters, like kinesin-1 (47, 48, 58, 59) and KIF17 (50), but also describes weakly processive mitotic motors. We speculate that the majority of kinesin family motors adhere to the same general kinetic scheme.

Previous studies that explored aspects of KIF15 motility at the single-molecule level reported results that differ from our own. Here, we determined the unloaded velocity and RL of KIF15 to be ∼550 nm·s^{-1} (Fig. 2*A*) and ∼130 nm (Fig. 4*B*), respectively. However, significantly slower velocities (76–190 nm·s^{-1}) but much longer RLs (400–5,000 nm) have been reported (32, 33, 35, 36). These discrepancies may be attributable to several factors:

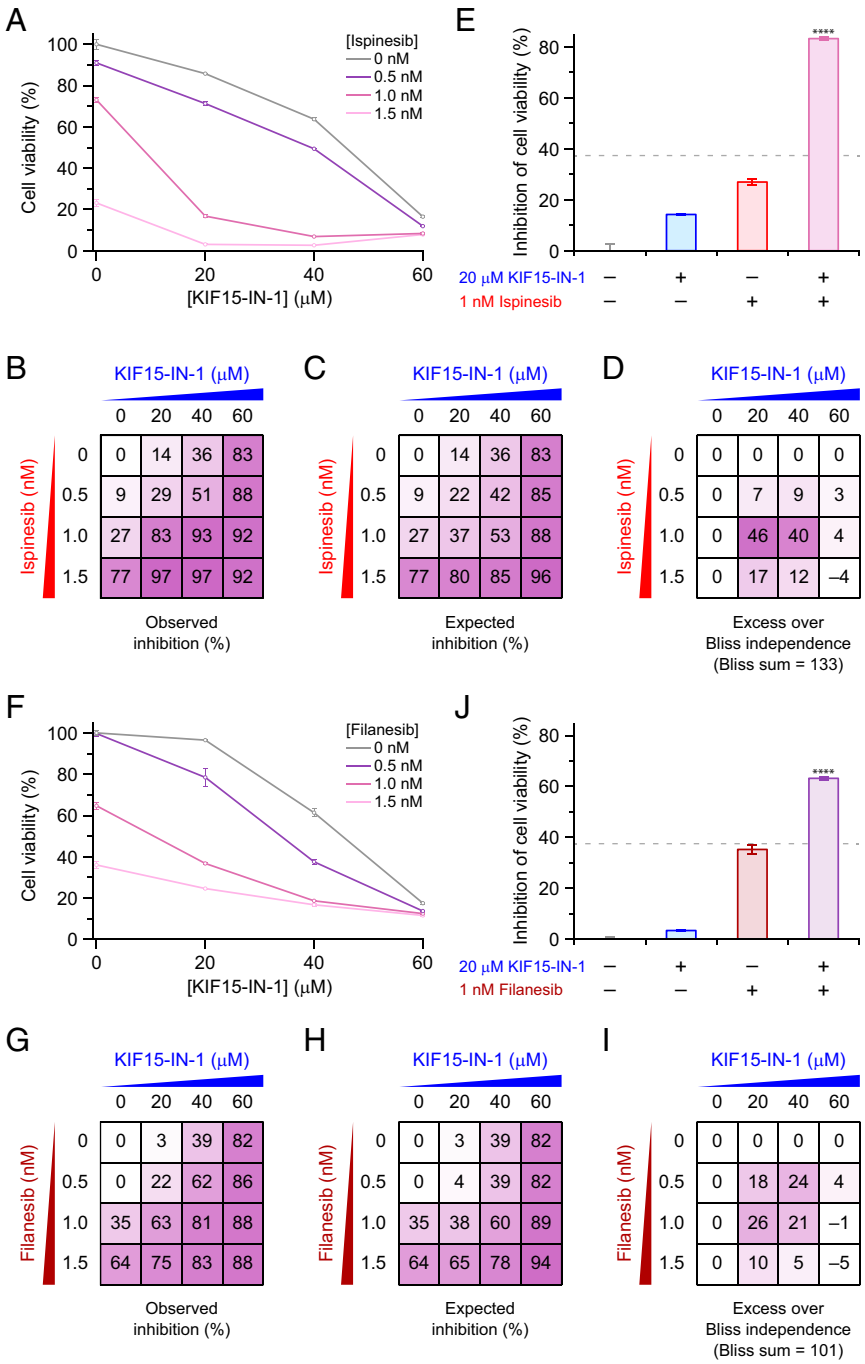

Fig. 6. Cell growth under combined inhibition of KIF15 and Eg5, quantified by mCherry fluorescence. Synergistic effects of KIF15 and Eg5 inhibitors were investigated with a HeLa cell proliferation assay in the presence of KIF15-IN-1 and either ispinesib (*A*–*E*) or filanesib (*F*–*J*). (*A* and *F*) Number of viable HeLa cells after 72 h of treatment (open circles; mean ± SE; $n = 3$) with pairwise combinations of KIF15 and Eg5 inhibitors (*Materials and Methods*), reported as a percentage relative to the control (no inhibitor). (*B* and *G*) Cell proliferation data from *A* and *F*, presented as a grid displaying the observed inhibition for each pairwise combination of drug doses (note that 0% cell viability corresponds to 100% inhibition). (*C* and *H*) Expected level of inhibition for a pair of inhibitors that act independent of one another (Bliss independence; *Materials and Methods*). (*D* and *I*) Grid displaying numerical differences between the observed and expected levels of inhibition (assuming independence) for each pairwise combination of drug doses, where positive values indicate synergy. (*E* and *J*) Strongest enhancement in the level of inhibition of viable cell number (bars; mean ± SE; $n = 3$), beyond that expected for no synergy (dotted horizontal lines), occurred when 20 μM KIF15-IN-1 was paired with 1 nM ispinesib (*E*; $^{****}P = 3 \times 10^{-6}$; one-tailed *t* test) or with 1 nM filanesib (*J*; $^{****}P = 8 \times 10^{-5}$; one-tailed *t* test) (also *SI Appendix*, Fig. S4).

i) Previously studied KIF15 motors lacked a 14-aa N-terminal segment of the motor domain (33, 36). N-terminal residues have been deemed important for force generation (69), and removing these might have impaired KIF15 motility.

ii) In our hands, recombinant KIF15 motors purified from bacteria had to be maintained in liquid nitrogen before use, because motility degraded within a day or two when motor proteins were flash-frozen in liquid nitrogen and later stored in a −80 °C freezer. Other laboratories, including our own, have traditionally stored their kinesin motor preparations at −80 °C, including those involved in previous studies of KIF15 constructs (33, 36). It seems possible that the activity

of those motors may have been compromised. As motors degrade, the likelihood that a motile KIF15 motor forms part of a small clump of motors increases dramatically, even though most of the motors still present in solution may remain in a dimeric, unclumped configuration. The inactivated motors in such clumps can function as brakes on motility, or as anchors to prevent MT dissociation, thereby leading to lower velocities and longer RLs than would be exhibited by individual, fully active dimers.

iii) Low-salt buffer conditions (32, 35) tend to stabilize electrostatic motor–MT interactions, thereby leading to reduced velocity and longer RL (70, 71).

iv) KIF15 motors prepared from cellular extracts may carry the uncontrolled presence of intracellular factors known to affect KIF15 motility, such as TPX2 (35).

The present findings are bolstered, however, by a recent study reporting an unloaded velocity of ∼500 nm·s^{-1} for KIF15 (34). This measurement, which agrees closely with our own, was obtained under similar buffer conditions, albeit at a higher assay temperature, using a full-length KIF15 construct that had been stored in liquid nitrogen.

In MT-gliding assays, we found not only that KIF15-IN-1 is a potent inhibitor of KIF15 motility (Fig. 5 *E* and *F*) but that KIF15 complexed with KIF15-IN-1 acts as a strong brake against Eg5-driven movement (Fig. 5 *G* and *H*). The precipitous drop in Eg5-driven velocity in the presence of inhibited KIF15 motors suggests that KIF15-IN-1 may stabilize an MT-bound state of KIF15, which Eg5 has difficulty overpowering in a mixed-motor assay. In contrast, the increase observed in gliding velocity with admixtures of KIF15 and Eg5, in response to the presence of either ispinesib or filanesib (Fig. 5 *G* and *H*), suggests that these inhibitors act to reduce the affinity of Eg5 to the MT, in agreement with earlier reports (72, 73). The fact that filanesib elicits a greater increase than ispinesib in gliding velocity with motor admixtures is also consistent with previous work, which demonstrated that Eg5–ispinesib complexes are more resistant to load-induced detachment from MTs than Eg5–filanesib complexes (73).

The ability of KIF15 to support MT gliding in vitro, even when vastly outnumbered by inhibited Eg5 motors (Fig. 5 *G* and *H*), helps to explain why KIF15 is able to facilitate resistance to Eg5 inhibitors in vivo. MT gliding powered by both of these mitotic motors was arrested only when they were separately inhibited, lending support to the proposal that a combination drug therapy targeting these motors may be a workable strategy for overcoming chemotherapeutic resistance to Eg5 inhibitors alone. The ability of Eg5 motors to rescue gliding under conditions of KIF15 inhibition suggests that such a combination therapy might also suppress any as-yet-undiscovered, Eg5-mediated mechanisms of resistance to KIF15 inhibition. The drug combination strategy is also supported by our results from cell culture, which show that drugs targeting KIF15 and Eg5 work synergistically to inhibit cancer cell proliferation (Fig. 6 and *SI Appendix*, Fig. S4).

Attempts to address the clinical failures of Eg5-targeted monotherapies have largely entailed either the development of increasingly potent inhibitors targeting the same motor, or pairing an Eg5 inhibitor with another (nonkinesin targeted) antimitotic drug (3, 8). The present study highlights the importance of understanding the molecular physiology of different kinesins and of exploring inhibitors that target additional mitotic kinesins, such as KIF15. More broadly, our results suggest that drug-development efforts involving molecular motors may benefit from a multiphasic approach.

Materials and Methods

Kinesin Expression and Purification. A truncated KIF15 gene coding for the first 700 aa of full-length human KIF15 (NCBI accession no. NP_064627) with a C-terminal 6× His-tag was synthesized commercially (Blue Heron Biotech) and inserted into a pET-15b vector (Novagen) between NcoI and XhoI restriction sites. We note that the truncated KIF15 construct polypeptide includes the secondary, noncatalytic MT-binding site, but does not include the autoinhibitory C-terminal portion of the stalk (33). Expression plasmids were transformed into BL21 (DE3) cells (New England BioLabs). A 1-L culture was grown in Terrific Broth supplemented with 4 mL·L^{-1} glycerol and 100 mg·L^{-1} ampicillin at 37 °C to OD_{600} = ∼0.6, induced with 0.5 mM isopropyl β-D-1-thiogalactopyranoside, and was subsequently grown at 19 °C for 8–9 h. Cells were pelleted, resuspended in lysis buffer (LB), and lysed in a prechilled French press (2,000 psi). The LB [50 mM Tris, 40 mM imidazole, 300 mM NaCl, 5 mM $MgCl_2$ (pH 7.9)] was supplemented immediately before use with 2 mM PMSF, 0.25 mM ATP, 0.5 mM DTT, and one tablet of cOmplete EDTA-free Protease Inhibitor Cocktail Tablets (Roche) per 50 mL. The clarified lysate was subjected to two rounds of centrifugation: first at 20,000 rpm (Sorvall SS-34 rotor) for 20 min at 4 °C and then at 50,000 rpm (Beckman Coulter MLA-55 rotor) for 1 h at 4 °C. Purification of His-tagged KIF15 from the lysate proceeded by passing the supernatant twice through 3 mL of Ni-NTA Agarose resin (Qiagen) in a gravity column. The resin was preequilibrated in wash buffer (WB) before the addition of the kinesin-containing lysate. The WB [30 mM Tris, 40 mM imidazole, 500 mM NaCl, 5 mM $MgCl_2$ (pH 7.9)] was supplemented with 75 μM ATP and 0.5 mM DTT immediately before use. High-salt conditions were used to ensure that KIF15 was purified as a dimer (32–34, 36). The resin was washed with 15 column volumes of WB before kinesin was eluted by passing elution buffer (EB) through the column. The EB consisted of WB with 300 mM imidazole. KIF15 concentrations in each column fraction were assessed spectroscopically, and the peak fractions were pooled. Sucrose was added to a final concentration of 10% wt/wt, after which the protein was aliquoted, flash-frozen, and stored in liquid nitrogen until thawing for use.

Separately, a truncated Eg5 gene coding for the first 513 aa of full-length human Eg5 (NCBI accession no. NP_004514) with a C-terminal 6× His-tag was generated by PCR amplification from an mCherry-Kinesin11-N-18 plasmid (no. 55067; Addgene). Primers were designed so that a sequence coding for the C-terminal 6× His-tag was introduced via PCR. The PCR product was inserted into a pET-15b vector (Novagen) between NcoI and XhoI restriction sites, and subsequently expressed and purified as described above.

Optical-Trapping Assay. The optical-trapping motility assay has been described (47, 53). Briefly, flow cells (channel volume = ∼10 μL) were assembled by using double-sided tape to attach plasma-cleaned coverslips coated with (3-aminopropyl)triethoxysilane (APTES) to glass microscope slides. MTs were cross-linked to the APTES surface using glutaraldehyde, after which the surface was passivated with BSA. His-tagged KIF15 motors were incubated with 440-nm-diameter polystyrene beads (Spherotech) precoated with Penta-His monoclonal antibodies (Qiagen) for 30 min at 4 °C before being introduced into the flow cells. Records of KIF15 translocation under unloaded conditions (0 pN) were obtained by video-tracking KIF15-coated beads moving along MTs (47, 53). An optical force clamp was used to study KIF15 motility under load by applying controlled loads to beads ferried along MTs by single molecules of KIF15 (47, 52, 53). Because KIF15 is highly temperature-sensitive, each flow cell was used for no more than 15 min after the addition of KIF15-coated beads, and each KIF15-bead incubation was typically used for no more than 2 h from the time when the KIF15 aliquot was removed from liquid nitrogen storage. All experiments were performed in a PEM80 assay buffer (AB) [80 mM piperazine-N,N′-bis(2-ethanesulfonic acid), 1 mM EGTA, 4 mM $MgCl_2$ (pH 6.9)] supplemented with 2 mM DTT, 10 μM Taxol, and 10 mg·mL^{-1} BSA, plus either ATP (Sigma) or ATPγS (Calbiochem) at the desired concentration. The AB was also supplemented with an oxygen-scavenging system (50 μg·mL^{-1} glucose oxidase, 12 μg·mL^{-1} catalase, 3 mg·mL^{-1} glucose) immediately before the introduction of bead-linked KIF15 motors into flow cells for experiments. All single-molecule measurements were obtained at an ambient temperature of 21 °C.

MT-Gliding Assay. Flow cells (channel volume = ∼10 μL) were assembled using double-sided tape to attach coverslips to glass microscope slides. The coverslip surface was incubated with a solution of 6× His monoclonal 3D5 antibodies (Invitrogen) in PEM80 for 5 min, after which the surface was passivated using passivation buffer (PB). The PB is AB with BSA replaced by 1 mg·mL^{-1} casein as the passivating agent. After incubating for 5 min, the flow cell was washed with motility buffer (MB), which contains 0.4 mg·mL^{-1} casein but is otherwise identical to PB. Next, an 80 nM (dimer) solution of KIF15 and/or Eg5 motors in MB was introduced and incubated for 5 min, after which the channel was washed with MB, optionally supplemented by kinesin inhibitors (KIF15-IN-1, ispinesib, and/or filanesib) at the desired concentrations. Finally, a solution of MTs in MB supplemented with an oxygen-scavenging system (50 μg·mL^{-1} glucose oxidase, 12 μg·mL^{-1} catalase, 3 mg·mL^{-1} glucose) and kinesin inhibitors

at the desired concentrations was introduced. Video recordings of MT gliding were recorded for up to 2 min per field of view. Each flow cell was used for no more than 15 min after the addition of MTs. No more than six slides were assessed before fresh solutions were prepared from frozen KIF15 or Eg5 aliquots. All MT-gliding measurements were obtained at an ambient temperature of 21 °C.

Kinesin inhibitors were obtained commercially: KIF15-IN-1 (catalog no. B3280; ApexBio), ispinesib (catalog no. 540810; Tocris), and filanesib (catalog no. 467610; Tocris).

Cell-Proliferation Assay. HeLa Kyoto cells constitutively expressing mCherry (HeLa-mCherry) were generated by transducing HeLa Kyoto cells with a lentiviral vector carrying mCherry driven by a CAG promoter, followed by fluorescence-activated cell sorting selection for fluorescence. In each well of two 24-well plates, 10,000 HeLa-mCherry cells in 1 mL of DMEM supplemented with 10% FBS were plated and grown at 37 °C, 5% CO_2 for 24 h. The growth medium was then replaced with 1 mL of DMEM and supplemented with 10% FBS and kinesin inhibitors at the desired concentrations. Live cell growth was monitored over 72 h using an IncuCyte ZOOM live-cell analysis system (Model 4459; Essen BioSciences).

For each well, images from 16 fields of view were acquired at intervals of 4 h using a 10× objective lens in a red fluorescence channel (excitation: 585 ± 20 nm, emission: 665 ± 40 nm, acquisition time: 0.35 s). The number of viable HeLa-mCherry cells in each well was quantified from the mCherry fluorescence signal (Fig. 6), averaged over the fields of view, using IncuCyte ZOOM software (Essen BioSciences). The fluorescence signal from cancer cells constitutively expressing mCherry has previously been shown to linearly depend on cell number (74). In parallel, phase-contrast images of the same 16 fields of view in each well were also acquired at 4-h intervals, which were then used to determine the number of viable cells on the basis of cell confluence (*SI Appendix*, Fig. S4), using IncuCyte ZOOM software (Essen BioSciences).

Optical-Trapping Data Analysis. The velocity of each single-molecule kinesin record was determined from the slope of a linear fit to the trace (47, 53); velocities obtained under identical loads and buffer conditions were then averaged. Variances in the individual stepping records were used to determine randomness, as described elsewhere (53, 55). As previously (47), the mean RL under unloaded conditions (0 pN) was obtained from an exponential fit to the histogram of individual KIF15 RLs. Bins with fewer than six counts were excluded from the fit, as was the first bin of the histogram. To determine the mean RL under load, individual RL measurements, x, that fell within the interval $x_1 < x < x_2$ were grouped separately from those that were longer than the upper limit, namely, $x > x_2$. The lower limit was set to $x_1 = 25$ nm for all loads, whereas the upper limit was set to $x_{2,-} = 150$ nm for hindering loads and $x_{2,+} = 90$ nm for assisting loads. Mean RLs (L) were calculated from the expression $L = (x_2 - x_1)/\ln(N_1/N_2 + 1)$, where N_1 is the number of runs in the $x_1 < x < x_2$ interval and N_2 is the number of runs longer than x_2. The SE (σ_L) was estimated from $\sigma_L = L\sqrt{N_1/(N_2(N_1+N_2))}/\ln(N_1/N_2+1)$. Finally, dissociation rates for both KIF15 and Eg5 were determined by dividing the mean velocity for each load and buffer condition by the corresponding mean RL.

Single-molecule Eg5 data, but not the fits derived here, are displayed in Figs. 2 and 4*B*, and *SI Appendix*, Fig. S2 and replotted from earlier work (20, 54).

Modeling the Kinesin Mechanochemical Cycle. The four-state kinetic scheme for the mechanochemical cycles of KIF15 and Eg5 (Fig. 3*A*) is identical to that developed for kinesin-2 motors (50), and the same analytical expressions hold for velocity (v) and randomness (r) as functions of applied load (F) and ATP concentration: These expressions are given in *SI Appendix*, *SI Materials and Methods*. The seven free parameters for KIF15 and Eg5 (Fig. 3*C*) were constrained by globally fitting the analytical expressions above to the velocity and randomness data for each motor separately (Fig. 2 and *SI Appendix*, Fig. S2 *A* and *B*). Global fitting was carried out using Igor Pro 6 (Wavemetrics).

MT-Gliding Data Analysis. The MT-gliding velocity was computed from displacements scored in video recordings (30 frames per second), by dividing the distance traveled by a given end of the MT between the starting and ending frames by the time elapsed between these frames. Velocities obtained under identical experimental conditions were then averaged (Fig. 5 *E*, *G*, and *H* and *SI Appendix*, Fig. S3).

Cell-Viability Data Analysis. Synergy between KIF15-IN-1 and either ispinesib or filanesib was assessed using the Bliss independence model, as used previously (64, 65). To establish whether a pair of inhibitor doses synergistically inhibits cell viability, it is first necessary to determine the expected inhibition for that pair of doses in the absence of synergy. The expected level of inhibition (Fig. 6 *C* and *H* and *SI Appendix*, Fig. S4 *C* and *H*) was calculated from the expression $F_{KIF15i} + F_{Eg5i} - (F_{KIF15i} \times F_{Eg5i})$, where F_{KIF15i} is the observed fractional growth inhibition for a KIF15 inhibitor dose in the absence of an Eg5 inhibitor and F_{Eg5i} is the observed fractional growth inhibition for an Eg5 inhibitor dose in the absence of a KIF15 inhibitor. Synergy was assessed by determining how much the observed level of inhibition (Fig. 6 *B* and *G* and *SI Appendix*, Fig. S4 *B* and *G*) for each pairwise condition exceeded the level of inhibition expected in the absence of any interaction (Fig. 6 *C* and *H* and *SI Appendix*, Fig. S4 *C* and *H*), where positive values indicate synergy (Fig. 6 *D* and *I* and *SI Appendix*, Fig. S4 *D* and *I*).

ACKNOWLEDGMENTS. We thank G.-Y. Chen and W. Hancock (Pennsylvania State University) for helpful suggestions about MT-gliding assays, D. Hogan (Stanford University) for software assistance, A. Savinov (Stanford University) for generous assistance in the latter stages of manuscript preparation, and M. Davidson (Florida State University) for providing the mCherry-Kinesin11-N-18 plasmid via Addgene. B.M. acknowledges the support of a Stanford Graduate Fellowship and NIH Training Grant 2T32GM008294. K.H. acknowledges the support of a Walter V. and Idun Berry Postdoctoral Fellowship. This work was supported by NIH Grants 5R37GM057035 (to S.M.B.), 1DP2HD084069 (to M.C.B.), and 5U01CA199216 (to M.C.B.), as well as a seed grant from Stanford Chemistry, Engineering, and Medicine for Human Health (to M.C.B.).

1. Hirokawa N, Noda Y, Tanaka Y, Niwa S (2009) Kinesin superfamily motor proteins and intracellular transport. *Nat Rev Mol Cell Biol* 10:682–696.
2. Verhey KJ, Hammond JW (2009) Traffic control: Regulation of kinesin motors. *Nat Rev Mol Cell Biol* 10:765–777.
3. Rath O, Kozielski F (2012) Kinesins and cancer. *Nat Rev Cancer* 12:527–539.
4. Welburn JP (2013) The molecular basis for kinesin functional specificity during mitosis. *Cytoskeleton (Hoboken)* 70:476–493.
5. Hirokawa N, Tanaka Y (2015) Kinesin superfamily proteins (KIFs): Various functions and their relevance for important phenomena in life and diseases. *Exp Cell Res* 334: 16–25.
6. Miki H, Setou M, Kaneshiro K, Hirokawa N (2001) All kinesin superfamily protein, KIF, genes in mouse and human. *Proc Natl Acad Sci USA* 98:7004–7011.
7. Miki H, Okada Y, Hirokawa N (2005) Analysis of the kinesin superfamily: Insights into structure and function. *Trends Cell Biol* 15:467–476.
8. Chandrasekaran G, Tátrai P, Gergely F (2015) Hitting the brakes: Targeting microtubule motors in cancer. *Br J Cancer* 113:693–698.
9. Myers SM, Collins I (2016) Recent findings and future directions for interpolar mitotic kinesin inhibitors in cancer therapy. *Future Med Chem* 8:463–489.
10. Ferenz NP, Gable A, Wadsworth P (2010) Mitotic functions of kinesin-5. *Semin Cell Dev Biol* 21:255–259.
11. Wojcik EJ, et al. (2013) Kinesin-5: Cross-bridging mechanism to targeted clinical therapy. *Gene* 531:133–149.
12. Enos AP, Morris NR (1990) Mutation of a gene that encodes a kinesin-like protein blocks nuclear division in A. nidulans. *Cell* 60:1019–1027.
13. Le Guellec R, Paris J, Couturier A, Roghi C, Philippe M (1991) Cloning by differential screening of a Xenopus cDNA that encodes a kinesin-related protein. *Mol Cell Biol* 11: 3395–3398.
14. Blangy A, et al. (1995) Phosphorylation by p34cdc2 regulates spindle association of human Eg5, a kinesin-related motor essential for bipolar spindle formation in vivo. *Cell* 83:1159–1169.
15. Cole DG, Saxton WM, Sheehan KB, Scholey JM (1994) A "slow" homotetrameric kinesin-related motor protein purified from Drosophila embryos. *J Biol Chem* 269: 22913–22916.
16. Kashina AS, et al. (1996) A bipolar kinesin. *Nature* 379:270–272.
17. Scholey JE, Nithianantham S, Scholey JM, Al-Bassam J (2014) Structural basis for the assembly of the mitotic motor kinesin-5 into bipolar tetramers. *eLife* 3:e02217.
18. Kapitein LC, et al. (2005) The bipolar mitotic kinesin Eg5 moves on both microtubules that it crosslinks. *Nature* 435:114–118.
19. Sawin KE, LeGuellec K, Philippe M, Mitchison TJ (1992) Mitotic spindle organization by a plus-end-directed microtubule motor. *Nature* 359:540–543.
20. Valentine MT, Fordyce PM, Krzysiak TC, Gilbert SP, Block SM (2006) Individual dimers of the mitotic kinesin motor Eg5 step processively and support substantial loads in vitro. *Nat Cell Biol* 8:470–476.
21. Roof DM, Meluh PB, Rose MD (1992) Kinesin-related proteins required for assembly of the mitotic spindle. *J Cell Biol* 118:95–108.
22. Houliston E, Le Guellec R, Kress M, Philippe M, Le Guellec K (1994) The kinesin-related protein Eg5 associates with both interphase and spindle microtubules during Xenopus early development. *Dev Biol* 164:147–159.
23. Sharp DJ, et al. (1999) The bipolar kinesin, KLP61F, cross-links microtubules within interpolar microtubule bundles of Drosophila embryonic mitotic spindles. *J Cell Biol* 144:125–138.
24. Mayer TU, et al. (1999) Small molecule inhibitor of mitotic spindle bipolarity identified in a phenotype-based screen. *Science* 286:971–974.

25. Tanenbaum ME, et al. (2009) Kif15 cooperates with Eg5 to promote bipolar spindle assembly. *Curr Biol* 19:1703–1711.
26. Vanneste D, Takagi M, Imamoto N, Vernos I (2009) The role of Hklp2 in the stabilization and maintenance of spindle bipolarity. *Curr Biol* 19:1712–1717.
27. Raaijmakers JA, et al. (2012) Nuclear envelope-associated dynein drives prophase centrosome separation and enables Eg5-independent bipolar spindle formation. *EMBO J* 31:4179–4190.
28. Sturgill EG, Ohi R (2013) Kinesin-12 differentially affects spindle assembly depending on its microtubule substrate. *Curr Biol* 23:1280–1290.
29. Sturgill EG, Norris SR, Guo Y, Ohi R (2016) Kinesin-5 inhibitor resistance is driven by kinesin-12. *J Cell Biol* 213:213–227.
30. Boleti H, Karsenti E, Vernos I (1996) Xklp2, a novel Xenopus centrosomal kinesin-like protein required for centrosome separation during mitosis. *Cell* 84:49–59.
31. Sueishi M, Takagi M, Yoneda Y (2000) The forkhead-associated domain of Ki-67 antigen interacts with the novel kinesin-like protein Hklp2. *J Biol Chem* 275: 28888–28892.
32. Drechsler H, McHugh T, Singleton MR, Carter NJ, McAinsh AD (2014) The Kinesin-12 Kif15 is a processive track-switching tetramer. *eLife* 3:e01724.
33. Sturgill EG, et al. (2014) Kinesin-12 Kif15 targets kinetochore fibers through an intrinsic two-step mechanism. *Curr Biol* 24:2307–2313.
34. Drechsler H, McAinsh AD (2016) Kinesin-12 motors cooperate to suppress microtubule catastrophes and drive the formation of parallel microtubule bundles. *Proc Natl Acad Sci USA* 113:E1635–E1644.
35. Mann BJ, Balchand SK, Wadsworth P (2017) Regulation of Kif15 localization and motility by the C-terminus of TPX2 and microtubule dynamics. *Mol Biol Cell* 28:65–75.
36. Reinemann DN, et al. (2017) Collective force regulation in anti-parallel microtubule gliding by dimeric Kif15 kinesin motors. *Curr Biol* 27:2810–2820.e6.
37. Wittmann T, Boleti H, Antony C, Karsenti E, Vernos I (1998) Localization of the kinesin-like protein Xklp2 to spindle poles requires a leucine zipper, a microtubule-associated protein, and dynein. *J Cell Biol* 143:673–685.
38. Wittmann T, Wilm M, Karsenti E, Vernos I (2000) TPX2, A novel xenopus MAP involved in spindle pole organization. *J Cell Biol* 149:1405–1418.
39. Gruss OJ, et al. (2002) Chromosome-induced microtubule assembly mediated by TPX2 is required for spindle formation in HeLa cells. *Nat Cell Biol* 4:871–879.
40. Sawin KE, Mitchison TJ (1995) Mutations in the kinesin-like protein Eg5 disrupting localization to the mitotic spindle. *Proc Natl Acad Sci USA* 92:4289–4293.
41. Valentine MT, Gilbert SP (2007) To step or not to step? How biochemistry and mechanics influence processivity in Kinesin and Eg5. *Curr Opin Cell Biol* 19:75–81.
42. McDonald A, Bergnes G, Morgans D (2004) Compounds, compositions and methods. US patent application publication US 20040053948A1 (March 18, 2004).
43. Lupas A, Van Dyke M, Stock J (1991) Predicting coiled coils from protein sequences. *Science* 252:1162–1164.
44. Svoboda K, Schmidt CF, Schnapp BJ, Block SM (1993) Direct observation of kinesin stepping by optical trapping interferometry. *Nature* 365:721–727.
45. Block SM, Asbury CL, Shaevitz JW, Lang MJ (2003) Probing the kinesin reaction cycle with a 2D optical force clamp. *Proc Natl Acad Sci USA* 100:2351–2356.
46. Jannasch A, Bormuth V, Storch M, Howard J, Schäffer E (2013) Kinesin-8 is a low-force motor protein with a weakly bound slip state. *Biophys J* 104:2456–2464.
47. Milic B, Andreasson JOL, Hancock WO, Block SM (2014) Kinesin processivity is gated by phosphate release. *Proc Natl Acad Sci USA* 111:14136–14140.
48. Andreasson JOL, et al. (2015) Examining kinesin processivity within a general gating framework. *eLife* 4:e07403.
49. Andreasson JOL, Shastry S, Hancock WO, Block SM (2015) The mechanochemical cycle of mammalian Kinesin-2 KIF3A/B under load. *Curr Biol* 25:1166–1175.
50. Milic B, Andreasson JOL, Hogan DW, Block SM (2017) Intraflagellar transport velocity is governed by the number of active KIF17 and KIF3AB motors and their motility properties under load. *Proc Natl Acad Sci USA* 114:E6830–E6838.
51. Visscher K, Schnitzer MJ, Block SM (1999) Single kinesin molecules studied with a molecular force clamp. *Nature* 400:184–189.
52. Valentine MT, et al. (2008) Precision steering of an optical trap by electro-optic deflection. *Opt Lett* 33:599–601.
53. Clancy BE, Behnke-Parks WM, Andreasson JOL, Rosenfeld SS, Block SM (2011) A universal pathway for kinesin stepping. *Nat Struct Mol Biol* 18:1020–1027.
54. Valentine MT, Block SM (2009) Force and premature binding of ADP can regulate the processivity of individual Eg5 dimers. *Biophys J* 97:1671–1677.
55. Schnitzer MJ, Block SM (1997) Kinesin hydrolyses one ATP per 8-nm step. *Nature* 388: 386–390.
56. Hackney DD (1994) Evidence for alternating head catalysis by kinesin during microtubule-stimulated ATP hydrolysis. *Proc Natl Acad Sci USA* 91:6865–6869.
57. Asenjo AB, Sosa H (2009) A mobile kinesin-head intermediate during the ATP-waiting state. *Proc Natl Acad Sci USA* 106:5657–5662.
58. Mickolajczyk KJ, et al. (2015) Kinetics of nucleotide-dependent structural transitions in the kinesin-1 hydrolysis cycle. *Proc Natl Acad Sci USA* 112:E7186–E7193.
59. Liu D, Liu X, Shang Z, Sindelar CV (2017) Structural basis of cooperativity in kinesin revealed by 3D reconstruction of a two-head-bound state on microtubules. *eLife* 6: e24490.
60. Klumpp LM, Hoenger A, Gilbert SP (2004) Kinesin's second step. *Proc Natl Acad Sci USA* 101:3444–3449.
61. Rice S, et al. (1999) A structural change in the kinesin motor protein that drives motility. *Nature* 402:778–784.
62. Yildiz A, Tomishige M, Gennerich A, Vale RD (2008) Intramolecular strain coordinates kinesin stepping behavior along microtubules. *Cell* 134:1030–1041.
63. Muretta JM, et al. (2015) The structural kinetics of switch-1 and the neck linker explain the functions of kinesin-1 and Eg5. *Proc Natl Acad Sci USA* 112:E6606–E6613.
64. Bliss CI (1939) The toxicity of poisons applied jointly. *Ann Appl Biol* 26:585–615.
65. Han K, et al. (2017) Synergistic drug combinations for cancer identified in a CRISPR screen for pairwise genetic interactions. *Nat Biotechnol* 35:463–474.
66. Carol H, et al. (2009) Initial testing (stage 1) of the kinesin spindle protein inhibitor ispinesib by the pediatric preclinical testing program. *Pediatr Blood Cancer* 53: 1255–1263.
67. Kasap C, Elemento O, Kapoor TM (2014) DrugTargetSeqR: A genomics- and CRISPR-Cas9-based method to analyze drug targets. *Nat Chem Biol* 10:626–628.
68. Chen GY, Mickolajczyk KJ, Hancock WO (2016) The kinesin-5 chemomechanical cycle is dominated by a two-heads-bound state. *J Biol Chem* 291:20283–20294.
69. Khalil AS, et al. (2008) Kinesin's cover-neck bundle folds forward to generate force. *Proc Natl Acad Sci USA* 105:19247–19252.
70. Shastry S, Hancock WO (2010) Neck linker length determines the degree of processivity in kinesin-1 and kinesin-2 motors. *Curr Biol* 20:939–943.
71. Thiede C, Lakämper S, Wessel AD, Kramer S, Schmidt CF (2013) A chimeric kinesin-1 head/kinesin-5 tail motor switches between diffusive and processive motility. *Biophys J* 104:432–441.
72. Lad L, et al. (2008) Mechanism of inhibition of human KSP by ispinesib. *Biochemistry* 47:3576–3585.
73. Chen GY, et al. (2017) Eg5 inhibitors have contrasting effects on microtubule stability and metaphase spindle integrity. *ACS Chem Biol* 12:1038–1046.
74. Busch S, et al. (2015) TGF-beta receptor type-2 expression in cancer-associated fibroblasts regulates breast cancer cell growth and survival and is a prognostic marker in pre-menopausal breast cancer. *Oncogene* 34:27–38.